



Cite this: *Phys. Chem. Chem. Phys.*,
2016, 18, 13423

On the nature of chemical bonding in the all-metal aromatic $[\text{Sb}_3\text{Au}_3\text{Sb}_3]^{3-}$ sandwich complex

Xue-Rui You,^a Wen-Juan Tian,^a Da-Zhi Li,^{*b} Ying-Jin Wang,^{ac} Rui Li,^a Lin-Yan Feng^a
and Hua-Jin Zhai^{*ad}

In a recent communication, an all-metal aromatic sandwich $[\text{Sb}_3\text{Au}_3\text{Sb}_3]^{3-}$ was synthesized and characterized. We report herein a density-functional theory (DFT) study on the chemical bonding of this unique cluster, which makes use of a number of computational tools, including the canonical molecular orbital (CMO), adaptive natural density partitioning (AdNDP), Wiberg bond index, and orbital composition analyses. The 24-electron, triangular prismatic sandwich is intrinsically electron-deficient, being held together *via* six Sb–Sb, three Au–Au, and six Sb–Au links. A standard, qualitative bonding analysis suggests that all CMOs are primarily located on the three $\text{Sb}_3/\text{Au}_3/\text{Sb}_3$ layers, three Au 6s based CMOs are fully occupied, and the three extra charges are equally shared by the two *cyclo*- Sb_3 ligands. This bonding picture is referred to as the zeroth order model, in which the cluster can be formally formulated as $[\text{Sb}_3^{1.5+}\text{Au}_3^{3-}\text{Sb}_3^{1.5+}]^{3-}$ or $[\text{Sb}_3^0\text{Au}_3^{3-}\text{Sb}_3^0]$. However, the system is far more complex and covalent than the above picture. Seventeen CMOs out of 33 in total involve remarkable Sb → Au electron donation and Sb ← Au back-donation, which are characteristic of covalent bonding and effectively redistribute electrons from the Sb_3 and Au_3 layers to the interlayer edges. This effect collectively leads to three Sb–Au–Sb three-center two-electron (3c–2e) σ bonds as revealed in the AdNDP analyses, despite the fact that not a single such bond can be identified from the CMOs. Orbital composition analyses for the 17 CMOs allow a quantitative understanding of how electron donation and back-donation redistribute the charges within the system from the formal $\text{Sb}_3^0/\text{Au}_3^{3-}$ charge states in the zeroth order model to the effective $\text{Sb}_3^{1.5-}/\text{Au}_3^0$ charge states, the latter being revealed from the natural bond orbital analysis.

Received 6th January 2016,
Accepted 14th April 2016

DOI: 10.1039/c6cp00101g

www.rsc.org/pccp

1. Introduction

A sandwich complex, by definition, normally refers to a chemical compound with a metal center bound to two arene (C_nH_n) ligands *via* haptic covalent bonds. Following the celebrated discovery of ferrocene, $(\text{C}_5\text{H}_5)_2\text{Fe}$, in the early 1950s,^{1,2} this field has been dominated by “metallocenes”, a special class of sandwich complexes. The metal center in sandwich complexes was extended to actinide in 1968, that is, in uranocene $\text{U}(\text{COT})_2$,³ whereas the arene ligands were incorporated with group 15 elements.⁴ Subsequently, the arene ligands were engineered and successfully made carbon-free, owing to the development in inorganic aromatic ring clusters in the gas phase, such as metalloid or metal rings. Among the discoveries is a carbon-free $[(\text{P}_5)_2\text{Ti}]^{2-}$ sandwich complex, which contains two aromatic P_5^- ligands.⁵ On the other

hand, in a series of synthetic studies,^{6–10} Murahashi and coworkers managed to insert a metal monolayer between two aromatic hydrocarbon ligands, resulting in a new class of sandwich complexes, which feature a multiple-metal-atom-sheet as the core.

The above-mentioned studies suggest intriguing opportunities to design and synthesize carbon-free sandwich complexes and, in particular, all-metal sandwiches. Computationally, a number of all-metal sandwich clusters with a single metal center were pursued lately, such as $[\text{Al}_4\text{TiAl}_4]^{2-}$,¹¹ $[\text{Sb}_5\text{TiSb}_5]^{2-}$,¹² and $[\text{Sb}_4\text{MSb}_4]^{2-}$ ($\text{M} = \text{Fe}, \text{Ru}, \text{Os}, \text{Co}, \text{Rh}, \text{Ir}; n = 1, 2$),¹³ which make use of aromatic Al_4^{2-} and Sb_5^- clusters as inorganic ligands.^{11–18} These all-metal sandwiches should be considered model systems, because the two metallic ligands are susceptible to coalescence. It is therefore not surprising that none of the prior all-metal sandwiches^{11–13} has been confirmed experimentally, either as synthetic bulk compounds or in the gas phase.

In a recent communication, Pan *et al.*¹⁹ reported for the first time a synthetic all-metal aromatic sandwich complex, $[\text{Sb}_3\text{Au}_3\text{Sb}_3]^{3-}$, which is crystallized in the form of $[\text{K}(\text{2.2.2})\text{crypt}][\text{Sb}_3\text{Au}_3\text{Sb}_3] \cdot (\text{0.5PPH}_3)_n$ ($n = \text{ethylenediamine}$). In this new sandwich, an Au_3 core is jammed between two aromatic, metallic *cyclo*- Sb_3 rings. Compared to ferrocene or metallocenes, the metal center

^a Nanocluster Laboratory, Institute of Molecular Science, Shanxi University, Taiyuan 030006, China. E-mail: hj.zhai@sxu.edu.cn

^b Department of Chemical Engineering, Binzhou University, Binzhou 256603, China. E-mail: ldz005@126.com

^c Department of Chemistry, Xinzhou Teachers University, Xinzhou 034000, China

^d State Key Laboratory of Quantum Optics and Quantum Optics Devices, Shanxi University, Taiyuan 030006, China

in the $[\text{Sb}_3\text{Au}_3\text{Sb}_3]^{3-}$ sandwich is extended from a single metal atom to an Au monolayer (albeit the smallest monolayer possible), and the arene ligands are switched to aromatic, metallic Sb_3 rings. These features make the $[\text{Sb}_3\text{Au}_3\text{Sb}_3]^{3-}$ sandwich highly unusual, which warrants a detailed computational study in order to fully understand its stability, as well as its nature of chemical bonding. The present work is intended to fulfill this purpose.

We show here that a qualitative bonding analysis of the canonical molecular orbitals (CMOs) for the $[\text{Sb}_3\text{Au}_3\text{Sb}_3]^{3-}$ all-metal sandwich reveals three features: (i) all CMOs are mainly located on the three $\text{Sb}_3/\text{Au}_3/\text{Sb}_3$ layers, and not a single CMO can be attributed primarily to the interlayer Sb–Au–Sb bonding; (ii) three Au 6s derived CMOs are fully occupied (with 6 electrons), hinting a major electron redistribution from the Sb_3/Sb_3 ligands to the central Au_3 layer; (iii) the three extra charges are equally shared by the two *cyclo*- Sb_3 ligands. The above bonding picture is referred to as the zeroth order model, at which a “standard”, routine chemical bonding analysis for a molecular system normally stops. In this model, the $[\text{Sb}_3\text{Au}_3\text{Sb}_3]^{3-}$ sandwich as a 24-electron system can be formulated as $[\text{Sb}_3^{1.5+}\text{Au}_3^{3-}\text{Sb}_3^{1.5+}]^{3-}$ or $[\text{Sb}_3^0\text{Au}_3^{3-}\text{Sb}_3^0]$, albeit the latter may be a bit misleading because it does not tell specifically where the three charges are situated. The zeroth order bonding model gives the formal charge states of Sb_3^0 and Au_3^{3-} in the sandwich. To obtain an in-depth understanding of the all-metal sandwich, one needs to go beyond the above model. The sandwich is shown to be held together *via* Sb → Au donation and Sb ← Au back-donation, involving 17 CMOs out of 33 in total in the system (12 valence CMOs and 21 “lone-pairs”). Certainly, this kind of bonding phenomenon can also exist in other sandwich complexes, such as $[\text{Pd}_4(\mu_4\text{-C}_9\text{H}_9)(\mu_3\text{-C}_8\text{H}_8)]^+$.²⁰ The sophisticated processes of donation and back-donation are characteristic of covalent bonding. The effect of these 17 CMOs is quantified *via* orbital composition analyses, which collectively redistribute as many as ~8 electrons back and forth between the $\text{Sb}_3/\text{Au}_3/\text{Sb}_3$ layers, leading to approximate $\text{Sb}_3^{1.5-}$ and Au_3^0 final charge states as well as minimal Au–Au bonding. The redistributed electrons are primarily accumulated along the interlayer edges, which are described vividly as three Sb–Au–Sb three-center two-electron (3c–2e) σ bonds according to the adaptive natural density

partitioning (AdNDP) analysis,²¹ despite the fact that not a single such bond can be identified from the CMOs.

2. Computational methods

The structural and electronic properties of the $[\text{Sb}_3\text{Au}_3\text{Sb}_3]^{3-}$ cluster have been studied using the density-functional theory (DFT).²² The DFT calculations were carried out at the PBE0^{23,24} and B3LYP levels, respectively, with the LANL2DZ,^{25,26} def2-TZVP,²⁷ and aug-cc-pVTZ-pp²⁸ basis sets. The calculated structural data indicate that the PBE0 method is superior to B3LYP for the current system. Note also that the size of the basis sets increases along this series. Thus, the PBE0/aug-cc-pVTZ-pp level of theory is considered to be the most reliable in the present work, and we will primarily discuss the computational data at this level.

To elucidate chemical bonding in the system, the CMO and AdNDP analyses were performed. Natural bond orbital (NBO)²⁹ analysis was also carried out to obtain the natural atomic charges and Wiberg bond indices. The AdNDP analyses were performed using the AdNDP program²¹ and all other calculations and analyses were carried out using the Gaussian 09 software package.³⁰

3. Results and discussion

3.1. Cluster structure of $[\text{Sb}_3\text{Au}_3\text{Sb}_3]^{3-}$

We fully optimized the D_{3h} $[\text{Sb}_3\text{Au}_3\text{Sb}_3]^{3-}$ sandwich structure using the PBE0 and B3LYP functionals, respectively, in combination with the LANL2DZ, def2-TZVP, and aug-cc-pVTZ-pp basis sets. The calculated bond distances and bond angles at all six levels of theory are summarized in Table 1, which are compared with the experimental data.¹⁹ A quick survey of the structural data clearly indicates that the PBE0 method performs better than B3LYP. For example, the calculated bond angles $\angle \text{SbAuSb}$ at PBE0 using the three basis sets are within -0.8° , $+0.2^\circ$, and -0.7° , respectively, of the experimental mean value ($\sim 178^\circ$); whereas those at B3LYP deviate by -3.4° , -5.0° , and -4.0° , respectively, from the experiment. Also, B3LYP appears to

Table 1 Optimized geometry of the all-metal sandwich $[\text{Sb}_3\text{Au}_3\text{Sb}_3]^{3-}$ cluster at the PBE0 and B3LYP levels, respectively, with the basis sets of aug-cc-pVTZ-pp, def2-TZVP, and LANL2DZ. The bond distances and bond angles are presented

Method		Bond distance (Å)			Bond angle (°)		
		Sb–Sb	Sb–Au	Au–Au	$\angle \text{SbSbSb}$	$\angle \text{SbAuSb}$	$\angle \text{AuAuAu}$
PBE0	aug-cc-pVTZ-pp ^a	2.96	2.67	3.07	60.00	177.18	60.00
	def2-TZVP	2.89	2.65	3.07	60.00	178.24	60.00
	LANL2DZ	2.99	2.69	3.10	60.00	177.27	60.00
B3LYP	aug-cc-pVTZ-pp	2.99	2.70	3.21	60.00	174.61	60.00
	def2-TZVP	2.93	2.69	3.21	60.00	173.02	60.00
	LANL2DZ	3.02	2.72	3.27	60.00	174.03	60.00
Exptl ^b		2.8615–2.8824	2.5919–2.6093	2.9179–2.9404	59.60–60.44	177.87–178.15	59.34–60.55

^a The PBE0/aug-cc-pVTZ-pp results are considered to be the most reliable of all computational data presented. ^b Experimental crystal data of $[\text{Sb}_3\text{Au}_3\text{Sb}_3]^{3-}$ from ref. 19.

produce significantly larger Au–Au/Sb–Au/Sb–Sb bond distances with respect to PBE0 as well as the experimental data, in particular for the Au–Au distance. In other words, the B3LYP geometry is less reliable in terms of bond distances. Overall, the larger aug-cc-pVTZ-pp basis set turns out to perform better than the small LANL2DZ basis set, at both the PBE0 and B3LYP levels. Based on the discussion, we should conclude that the PBE0/aug-cc-pVTZ-pp level of theory works pretty well for the $[\text{Sb}_3\text{Au}_3\text{Sb}_3]^{3-}$ system (and the PBE0/def2-TZVP method appears to perform just as good), which faithfully reproduces the experimental cluster structure.

The ultimate optimized structure of $[\text{Sb}_3\text{Au}_3\text{Sb}_3]^{3-}$ at the PBE0/aug-cc-pVTZ-pp level is illustrated in Fig. 1. The calculated bond angles in the Au_3 ring, as well as in *cyclo*- Sb_3 ligands, are 60° , consistent with the D_{3h} symmetry of the all-metal sandwich. The $\angle \text{SbAuSb}$ bond angle is calculated to be 177.18° (experimental data: 177.87 – 178.15°),¹⁹ indicating that the Sb–Au–Sb edges in the sandwich are virtually linear. The calculated Sb–Sb, Sb–Au, and Au–Au distances are 2.96, 2.67, and 3.07 Å, respectively, which are close to and slightly larger than the experimental data (Table 1). It should be stressed that the current calculations of the gas-phase cluster do not take into account the electrostatic stabilization effect of the counterions as presented in the synthetic $[\text{Sb}_3\text{Au}_3\text{Sb}_3]^{3-}$ complex.¹⁹ Such calculations are anticipated to produce Au–Au/Sb–Au/Sb–Sb distances that are slightly greater than the experimental measurements,³¹ due to the intrinsic intramolecular coulomb repulsion between three extra charges in the gas-phase cluster.

According to the latest recommended covalent radii by Pyykkö,^{32,33} the upper limits for typical distances of Sb–Sb, Sb–Au, and Au–Au single bonds are 2.80, 2.64, and 2.48 Å, respectively. Thus, the Sb–Sb and Sb–Au bonds in $[\text{Sb}_3\text{Au}_3\text{Sb}_3]^{3-}$ are comparable to single bonds. In particular, the Sb–Au distances suggest that bonding interaction between the $\text{Sb}_3/\text{Au}_3/\text{Sb}_3$ layers in the sandwich is remarkably strong. In contrast, the

Au–Au bonding is only minimal in the system. Indeed, the calculated and experimental Au–Au distances (~ 3 Å) are significantly larger than those of a single bond. These are actually close to the magic Au–Au distance for aurophilicity,^{34–37} which describes the unique closed-shell interaction between two Au(I) d^{10} centers in Au compounds. Aurophilicity is dispersive in nature like van der Waals interactions, but it is enhanced to 7–12 kcal mol^{−1} and becomes comparable in strength to hydrogen bonds due to relativistic effects of Au.³⁵ Despite the fact that the Au centers in $[\text{Sb}_3\text{Au}_3\text{Sb}_3]^{3-}$ are not in the Au(I) state (see below), the Au–Au interaction in the sandwich appears to be dominated by aurophilicity.

Among the alternative structures of interest for the $[\text{Sb}_3\text{Au}_3\text{Sb}_3]^{3-}$ sandwich, as requested by one reviewer, is a more closely packed, staggered conformation, which differs from that in Fig. 1 by an in-plane twist of the interlayer Au_3 by 60° . This staggered structure also has D_{3h} symmetry. Our preliminary calculations at the PBE0/aug-cc-pVTZ-pp level indicate, however, that the new structure is not a true minimum and it is estimated to be at least 10 kcal mol^{−1} higher in energy, consistent with the fact that this conformation is not present in the synthetic compounds.¹⁹

3.2. Chemical bonding: all-metal sandwich $[\text{Sb}_3\text{Au}_3\text{Sb}_3]^{3-}$ as a 24-electron system

The CMOs are fundamental in understanding the nature of bonding in a molecular system. Considering the atomic electron configurations of $5s^25p^3$ for Sb and $5d^{10}6s^1$ for Au, the $[\text{Sb}_3\text{Au}_3\text{Sb}_3]^{3-}$ cluster has 66 valence electrons (including the three extra electrons). All 33 occupied CMOs of these electrons are illustrated in Fig. 2 and 3.

We can start the bonding analysis with a triangular, model Sb_3^{3-} cluster, whose CMOs are shown in Fig. 4. It has three subsets of CMOs: three Sb 5s derived CMOs (HOMO–5 and HOMO–4/HOMO–4', where HOMO stands for the highest occupied molecular orbital), as well as six Sb 5p derived ones (HOMO–3 and HOMO–1/HOMO–1' as one subset, and HOMO–2 and HOMO/HOMO' as another subset). In a D_{3h} structure, each atomic orbital (AO) can combine into three CMOs, that is, one completely bonding CMO and two degenerate, partially bonding/antibonding CMOs. When all three CMOs are fully occupied, they can in turn be transformed to three lone-pairs or three 2c–2e bonds. In the case of the Sb_3^{3-} cluster, the first three CMOs (Fig. 4(a)) are readily transformed to three 2c–2e Sb–Sb p_π bonds, the next three (Fig. 4(b)) to three 2c–2e Sb–Sb p_σ bonds, and the last three (Fig. 4(c)) to three Sb 5s lone-pairs.

In the $[\text{Sb}_3\text{Au}_3\text{Sb}_3]^{3-}$ sandwich, Sb 5s AOs in each *cyclo*- Sb_3 ligand combine to form three orbitals. Each specific orbital can further combine constructively and destructively between the two ligands, generating a pair of CMOs in the sandwich. All six Sb 5s² based CMOs of $[\text{Sb}_3\text{Au}_3\text{Sb}_3]^{3-}$ are shown in Fig. 2(a), which are practically 6c–2e in nature. These CMOs consist of three constructive/destructive pairs as mentioned above: HOMO–21/HOMO–20, HOMO–19'/HOMO–18', and HOMO–19/HOMO–18. At the zero-order approximation, one pair can

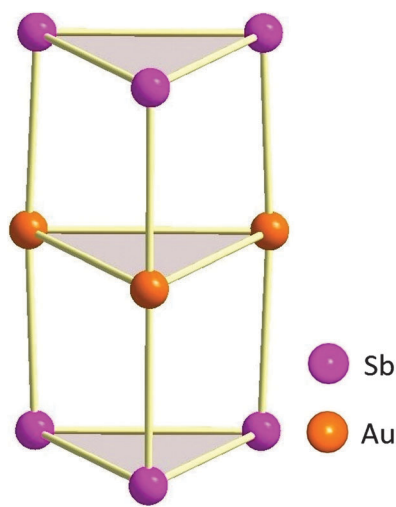


Fig. 1 Optimized D_{3h} structure of $[\text{Sb}_3\text{Au}_3\text{Sb}_3]^{3-}$ at the PBE0/aug-cc-pVTZ-pp level. Bond distances (in Å): Sb–Sb, 2.96; Au–Au, 3.07; Sb–Au, 2.67. Bond angles (in degrees): $\angle \text{SbSbSb}$, 60° ; $\angle \text{AuAuAu}$, 60° ; $\angle \text{SbAuSb}$, 177.18° .

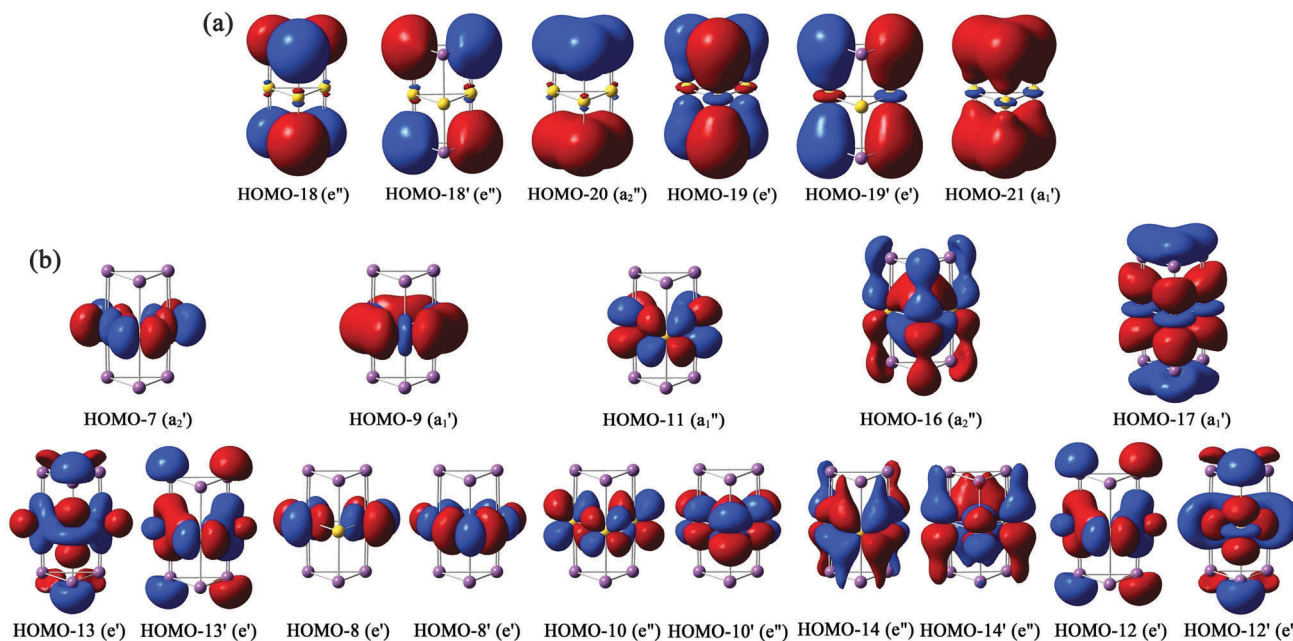


Fig. 2 Pictures of occupied canonical molecular orbitals (CMOs) of $[\text{Sb}_3\text{Au}_3\text{Sb}_3]^{3-}$ that are associated with (a) six Sb $5s^2$ lone-pairs and (b) fifteen Au $5d^{10}$ lone-pairs, calculated at the PBE0/aug-cc-pVTZ-pp level. These CMOs consume 42 electrons out of 66 in total in the system.

be recombined to two orbitals, each on one Sb_3 . In other words, the six CMOs of the sandwich (Fig. 2(a)) are equivalent to two sets of CMOs in Fig. 4(c), one set for each *cyclo*- Sb_3 ligand. Consequently, the six CMOs may be collectively transformed to six Sb $5s$ lone-pairs, one for every Sb center. Similarly, the CMOs shown in Fig. 2(b) are approximated to 15 Au $5d$ lone-pairs, 5 for each Au center (d_{xy} , d_{yz} , d_{xz} , $d_{x^2-y^2}$, and d_{z^2}). Therefore, the 21 CMOs shown in Fig. 2 correspond to the Sb $5s^2$ and Au $5d^{10}$ lone-pairs, which consume 42 electrons out of 66 in total in the system (that is, $\sim 63\%$). It is stressed that “lone-pairs” are only an oversimplified view.

With Sb $5s^2$ and Au $5d^{10}$ lone-pairs excluded, the $[\text{Sb}_3\text{Au}_3\text{Sb}_3]^{3-}$ sandwich is bound *via* 24 electrons: three $5p$ electrons from each Sb, one $6s$ electron from each Au, and three extra electrons. The 24-electron system of $[\text{Sb}_3\text{Au}_3\text{Sb}_3]^{3-}$ is electron-deficient, which has six Sb–Sb, three Au–Au, and six Sb–Au links. The 12 corresponding CMOs are depicted in Fig. 3, which underlie the stability of the all-metal sandwich. The six Sb $5p$ based σ CMOs are shown in Fig. 3(a). Here the three in the first row are a constructive combination between two Sb_3 ligands, whereas those in the second row are their corresponding destructive combination. These readily recombine to form two sets of p_σ orbitals (Fig. 4(b)) for the *cyclo*- Sb_3 ligands and further to form six $2c-2e$ Sb–Sb p_σ bonds. In short, the six CMOs in Fig. 3(a) correspond to six Sb–Sb p_σ bonds in the *cyclo*- Sb_3 ligands.

As for the Au $6s$ based CMOs, three can be identified, HOMO–15/HOMO–2/HOMO–2' (Fig. 3(b)), being fully occupied with six electrons. This observation suggests that the two *cyclo*- Sb_3 ligands need to contribute three electrons to the Au $6s$ based bonding, at least formally. The remaining three CMOs (Fig. 3(c)) are responsible for p_π bonding between two Sb_3 ligands, which are the only delocalized bonds in the system. Note that the HOMO in

$[\text{Sb}_3\text{Au}_3\text{Sb}_3]^{3-}$ is doubly degenerate and based on two Sb_3 ligands, where the three extra electrons are supposed to locate. Thus, in a zeroth order model the sandwich should be formulated as $[\text{Sb}_3^{1.5+}\text{Au}_3^{3-}\text{Sb}_3^{1.5+}]^{3-}$, in which two Sb_3 ligands provide three electrons to Au_3 for its $6s$ based CMOs (Fig. 3(b)) and the three extra electrons in turn exactly compensate the Sb_3 ligands for their electron losses (Fig. 3(c)). In this picture, the Au and Sb centers in $[\text{Sb}_3\text{Au}_3\text{Sb}_3]^{3-}$ appear to be in the formal charge states of Au^- and Sb^0 . It may be stated that the zeroth order model has a major ionic component due to the redistribution of three electrons from the Sb_3/Sb_3 ligands to the Au_3 $6s$ based CMOs; see below for further quantitative data of the electron redistribution.

In terms of the electronic properties of the $[\text{Sb}_3\text{Au}_3\text{Sb}_3]^{3-}$ sandwich, the original work¹⁹ reported a large energy gap of 3.08 eV between the HOMO and the lowest unoccupied molecular orbital (LUMO) of $[\text{Sb}_3\text{Au}_3\text{Sb}_3]^{3-}$ at the PBE0/def2-TZVP level. We can basically repeat the HOMO–LUMO gap, 3.04 eV to be exact. However, with the larger basis set of aug-cc-pVTZ-pp, the calculated energy gap is much smaller, 1.15 eV at B3LYP and 1.41 eV at PBE0, the latter value being considered to be the most reliable (see Section 2).^{38,39} Thus the all-metal sandwich cluster may exhibit sort of semiconducting property.

3.3. Aromaticity and nucleus-independent chemical shift (NICS)

Of all 33 CMOs in Fig. 2 and 3, only the HOMO/HOMO' and HOMO–4 (Fig. 3(c)) are truly delocalized. The three CMOs are primarily six-centered in nature, representing the destructive combination between two *cyclo*- Sb_3 ligands, which cannot be further transformed to three-center bonds, or $2c-2e$ bonds, or lone-pairs. However, their origin can be straightforwardly

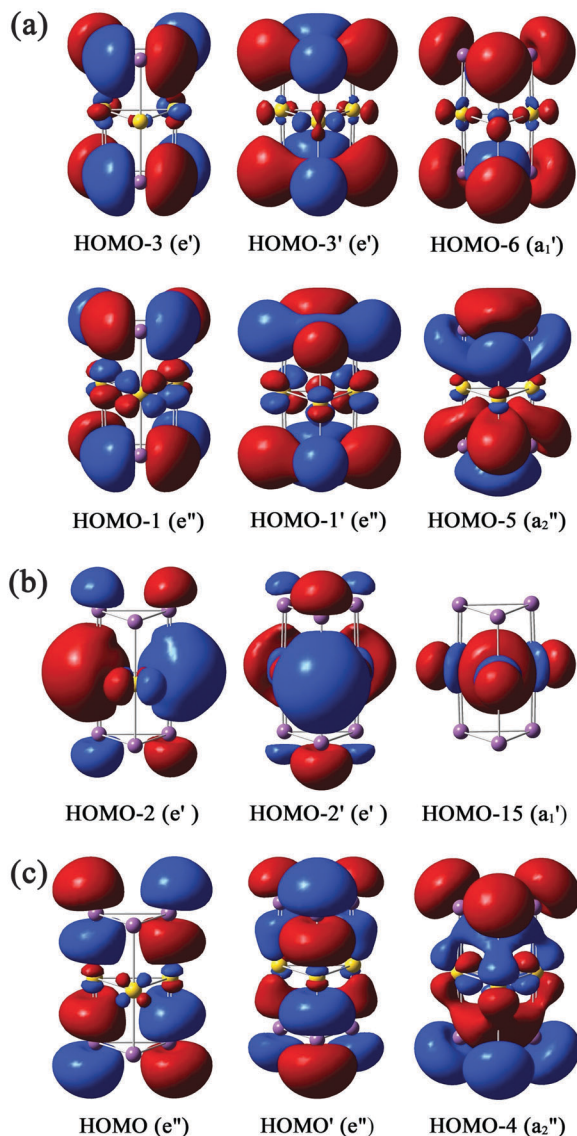


Fig. 3 Pictures of all CMOs in $[\text{Sb}_3\text{Au}_3\text{Sb}_3]^{3-}$ calculated at the PBE0/aug-cc-pVTZ-pp level, with the exclusion of the Sb $5s^2$ and Au $5d^{10}$ lone-pairs (Fig. 2). These CMOs involve the Sb $5p^3$ and Au $6s^1$ electrons, as well as three extra charges in the cluster, collectively making a 24-electron system.

traced back to the model Sb_3^{3-} cluster. Indeed, the CMOs in Fig. 3(c) show exact one-to-one correspondence to those in Fig. 4(a), except that the former CMOs are two-layer stacks of orbitals from the two Sb_3 ligands. Thus, the six-center six-electron ($6c-6e$) π system in $[\text{Sb}_3\text{Au}_3\text{Sb}_3]^{3-}$ (Fig. 3(c)) can be cut in halves, leading to two effective $3c-3e$ π subsystems.

Such a $3c-3e$ π subsystem possesses three orbitals that are similar to those in Fig. 4(a), one being delocalized and completely bonding and two being degenerate and partially bonding/antibonding. The uniqueness in the $3c-3e$ π subsystem is that all three orbitals are half-occupied. This bonding situation is closely in the spirit of a $3c-4e$ $\pi\pi^*$ triplet species, which is known to be aromatic following the reversed $4n$ Hückel rule for aromaticity.⁴⁰ The only difference between the present, equivalent $3c-3e$ Sb_3 π subsystem and a $3c-4e$ $\pi\pi^*$ triplet species is

that the completely bonding orbital in the former is also half occupied, whereas it is fully occupied in the latter. Note that full- or half-occupation of the delocalized, completely bonding orbital does not alter the nature of aromaticity in a system. Thus the $[\text{Sb}_3\text{Au}_3\text{Sb}_3]^{3-}$ all-metal sandwich complex is π aromatic.⁴¹

The NICS is widely accepted as a computational measure of aromaticity.^{42,43} We have calculated the $\text{NICS}(1)_{zz}$ at 1 Å above the center of the *cyclo*- Sb_3 ligands in $[\text{Sb}_3\text{Au}_3\text{Sb}_3]^{3-}$, which amounts to -34.99 ppm at the PBE0/aug-cc-pVTZ-pp level, confirming the remarkably strong π aromaticity for the all-metal sandwich complex. For comparison, the prototypical π aromatic benzene molecule has a $\text{NICS}(1)_{zz}$ value of -30.30 ppm at the PBE0/aug-cc-pVTZ level.

3.4. The nature of edge Sb–Au–Sb interactions in $[\text{Sb}_3\text{Au}_3\text{Sb}_3]^{3-}$: electron donation and back-donation, orbital compositions, and natural atomic charges

The above bonding analyses suggest that $[\text{Sb}_3\text{Au}_3\text{Sb}_3]^{3-}$ is essentially a triple-layered sandwich complex. The 24-electron system (Fig. 3) formally consists of 12 electrons for six $2c-2e$ Sb–Sb σ bonds, 6 electrons for Au $6s$ based CMOs, and delocalized 6π electrons. The latter are situated in the two *cyclo*- Sb_3 ligands, rendering π aromaticity for the all-metal sandwich. The CMO analyses also indicate that the sandwich should be formulated as $[\text{Sb}_3^{1.5+}\text{Au}_3^{3-}\text{Sb}_3^{1.5+}]^{3-}$ in the zeroth order model, which possesses formal Sb^0 and Au^- centers. However the NBO analyses (Table 2) at all six levels of theory consistently offer a different picture: the interlayer Sb–Au bonding appears to be strong with a Wiberg bond order of 0.71 at the PBE0/aug-cc-pVTZ-pp level, and the Au–Au bond order is only 0.23. These bond orders are in line with their bond distances (see Section 3.1). Furthermore, the natural atomic charges from NBO analysis are -0.493 $|e|$ for Sb and -0.014 $|e|$ for Au, which are also in sharp contrast to those in the zeroth order model.

Therefore, a couple of crucial issues remain to be addressed in the all-metal sandwich: how can three Au $6s$ based CMOs offer only minimal Au–Au bonding? How to reconcile the formal Sb^0 and Au^- charge states in the zeroth order model and those of $\text{Sb}^{0.5-}$ and Au^0 from the NBO analysis? What is the nature of interlayer Sb–Au–Sb bonding? The key to these questions lies in the quantitative composition analyses of the CMOs.

A closer examination of the CMOs in Fig. 2 and 3 reveals that, while every CMO can be clearly assigned to either the Au_3 layer or the Sb_3/Sb_3 ligands, the majority of CMOs possess also a secondary component. Such secondary components serve to redistribute electrons, *via* sophisticated Sb \rightarrow Au donation and Sb \leftarrow Au back-donation, in between the $\text{Sb}_3/\text{Au}_3/\text{Sb}_3$ layers and from the layers to the interlayer Sb–Au–Sb edges. It is such secondary components that play the vital role in binding three $\text{Sb}_3/\text{Au}_3/\text{Sb}_3$ layers for a sandwich complex. Table 3 summarizes the results of orbital composition analyses for selected CMOs, whose secondary component is close to 10% or larger. The electron redistribution in the system can be classified into four categories. As a starting point, the metal centers in the sandwich are in the Sb^0 and Au^0 charge states.

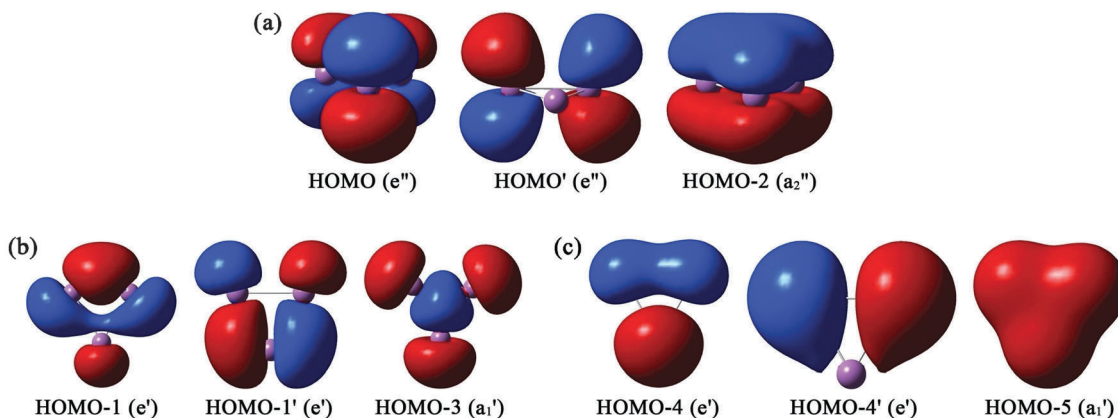


Fig. 4 Pictures of occupied CMOs of the *cyclo-Sb₃³⁻* model cluster at the PBE0/aug-cc-pVTZ-pp level.

Table 2 Calculated Wiberg bond indices and natural atomic charges *via* natural bond orbital (NBO) analysis at the PBE0 and B3LYP levels, respectively, with basis sets of aug-cc-pVTZ-pp, def2-TZVP, and LANL2DZ

Method		Wiberg bond index			Natural charge ^a (<i> e </i>)	
		Sb–Sb	Sb–Au	Au–Au	Sb	Au
PBE0	aug-cc-pVTZ-pp ^b	0.93	0.71	0.23	−0.493	−0.014
	def2-TZVP	0.94	0.69	0.22	−0.551	0.102
	LANL2DZ	0.94	0.70	0.20	−0.516	0.031
B3LYP	aug-cc-pVTZ-pp	0.93	0.68	0.18	−0.486	−0.028
	def2-TZVP	0.94	0.68	0.19	−0.543	0.087
	LANL2DZ	0.94	0.67	0.17	−0.507	0.013

^a Charge per Au or Sb atom. ^b The PBE0/aug-cc-pVTZ-pp results are considered to be the most reliable of all computational data presented.

Category 1 shows that three extra electrons in $[\text{Sb}_3\text{Au}_3\text{Sb}_3]^{3-}$ are faithfully distributed on the two Sb_3 ligands (by $\sim 2.9 |e|$; Table 3). Category 2 describes the major electron transfer from Sb to Au, formally by 3 electrons, *via* the occupation of HOMO–2 and HOMO–2' (Fig. 3(b)). The above two processes lead to the formulation of $[\text{Sb}_3^{1.5+}\text{Au}_3^{3-}\text{Sb}_3^{1.5+}]^{3-}$ for the sandwich in the zeroth order model, as well as the formal Sb^0 and Au^- charge states. However, category 2 actually only involves a charge transfer of $\sim 1.8 |e|$ (compared to 3.0 $|e|$ formally), because HOMO–2 and HOMO–2' contain merely $\sim 60\%$ Au s/p/d.

Categories 3 and 4 show the secondary Sb \rightarrow Au donation and Sb \leftarrow Au back-donation processes, which involve 7 and 10 CMOs, respectively (Table 3). For the 7 CMOs associated with the Sb \rightarrow Au donation, the Au s/p/d component ranges from $\sim 10\%$ to 26%, collectively resulting in the donation of $\sim 2.3 |e|$ to Au. On the other hand, the 10 CMOs for Sb \leftarrow Au back-donation have a Sb s/p component from 10% up to 41%, which manage to back-donate a total of $\sim 3.7 |e|$ to Sb. Categories 3 and 4 demonstrate the powerfulness of electron donation and back-donation *via* multiple CMOs (17 in total). While individually each CMO only redistributes as little as 0.2 $|e|$, their collective effect is to move up to 6 $|e|$ back and forth between the $\text{Sb}_3/\text{Au}_3/\text{Sb}_3$ layers. To be specific, Au_3 accepts 1.85 $|e|$ *via* its Au 6s based HOMO–2/HOMO–2' from the Sb_3 ligands

(category 2) and $\sim 2.3 |e|$ *via* 7 other CMOs (category 3), whereas it back-donates $\sim 3.7 |e|$ to the Sb_3 ligands *via* 10 CMOs (category 4), ultimately making the Au_3 layer almost neutral.

Electron donation and back-donation are known for covalent bonding interactions, which help bound the three metallic layers together as a sandwich. It is stressed that 11 out of the 17 CMOs associated with categories 3 and 4 are in fact portion of Sb 5s² and Au 5d¹⁰ lone-pairs (Fig. 2), which contribute to the redistribution of $\sim 4.1 |e|$ back and forth (that is, almost 70% of the total), suggesting that many of the Sb 5s² and Au 5d¹⁰ “lone-pairs” are not pure.

The net effect of the four categories of processes is to reach the final charge states of $\text{Sb}^{0.42-}$ and $\text{Au}^{0.16-}$ (Table 3) in the sandwich, which are very different from those in the zeroth order picture (Sb^0 and Au^-) but remarkably close to the NBO data ($\text{Sb}^{0.493-}$ and $\text{Au}^{0.014-}$; Table 2). It may be argued that the donation and back-donation in categories 2 through 4 are mainly accumulated at the interlayer Sb–Au–Sb edges, hinting at an Sb–Au bond order of larger than 0.6 (about $\sim 7.8 |e|$ for six Sb–Au links), which is close to the NBO bond order (0.71; Table 2).

The nature of the approximate Au^0 final charge state from orbital composition analyses (Table 3), as well as from NBO analysis (Table 2), also helps explain why the Au–Au bonding is minimal in the all-metal sandwich. As an estimate, the six electrons in HOMO–2/HOMO–2'/HOMO–15 (Fig. 3(b)) contain 2.35 $|e|$ of the Sb component (Table 3), which contributes to portion of the Sb–Au interactions. Assume that the Au 6s component contributes a similar amount to the Sb–Au interaction, then these three CMOs only have $\sim 1.3 |e|$ for Au–Au interaction within the Au_3 layer (that is, a bond order of ~ 0.2). While this estimation is too simplified, it is in good agreement with the calculated Wiberg bond order of 0.23 at the PBE0/aug-cc-pVTZ-pp level (Table 2).

3.5. On the three effective Sb–Au–Sb three-center two-electron (3c–2e) σ bonds

The AdNDP analysis²¹ can provide a valuable, alternative view of the chemical bonding in a molecular system. As an extension of the NBO analysis, AdNDP represents the electronic structure of a molecule in terms of *n*-center two-electron (*nc*–2e) bonds,

Table 3 Charge redistribution in the all-metal sandwich $[\text{Sb}_3\text{Au}_3\text{Sb}_3]^{3-}$ cluster via the composition analysis of canonical molecular orbitals (CMOs) at the PBE0/aug-cc-pVTZ-pp level. Only the CMOs with an electron redistribution of around 10% or greater are included. Some 19 CMOs participate in these processes

Channel	CMO	Au (%)			Sb (%)		Electron transfer ^a ($ e $)	
		s	p	d	s	p	Au ₃	Sb ₃ /Sb ₃
Extra charges	HOMO/HOMO'	—	—	—	—	97.0	-0.09	-2.91 ^b
Major Sb → Au	HOMO-2/HOMO-2'	31.2	9.6	20.6	2.0	36.2	-1.85 ^c	+1.85
Sb → Au	HOMO-20	—	12.8	—	73.1	13.0	-0.26	+0.26
	HOMO-19	8.1	1.5	16.1	66.2	8.0	-0.51	+0.51
	HOMO-19'	8.1	1.5	16.1	66.2	7.9	-0.52	+0.52
	HOMO-21	9.4	2.3	5.1	71.3	11.3	-0.34	+0.34
	HOMO-1	—	—	9.5	1.3	88.3	-0.19	+0.19
	HOMO-1'	—	—	9.6	1.3	87.8	-0.19	+0.19
	HOMO-4	—	—	14.0	4.8	79.8	-0.28	+0.28
Sb ← Au	HOMO-2/HOMO-2'	31.2	9.6	20.6	2.0	36.2	+0.38	-0.38 ^d
	HOMO-10'	20.2	1.8	66.5	—	11.0	+0.23	-0.23
	HOMO-16	—	—	84.2	4.1	11.3	+0.31	-0.31
	HOMO-14	—	—	89.3	1.0	9.4	+0.21	-0.21
	HOMO-14'	—	—	89.4	1.0	9.3	+0.21	-0.21
	HOMO-17	—	—	86.9	—	10.2	+0.21	-0.21
	HOMO-12	1.7	—	64.0	12.2	21.5	+0.68	-0.68
	HOMO-12'	1.7	—	64.0	12.2	21.5	+0.68	-0.68
	HOMO-15	20.8	4.4	32.8	6.1	35.4	+0.83	-0.83
Total							-0.49	-2.51
Average ^e (charge per atom)							-0.16	-0.42

^a Electron gain for Sb₃/Au₃/Sb₃ is denoted as “-”, whereas electron loss is denoted as “+”. ^b Only three out of four electrons in HOMO/HOMO' are due to the extra charges. ^c Only three out of four electrons (75%) in HOMO-2/HOMO-2' are associated with the major Sb → Au electron transfer.

^d One out of four electrons (25%) in HOMO-2/HOMO-2' is originally Au 6s based, which involves partial Sb ← Au electron transfer. ^e A standard bonding analysis of a molecular system assigns all CMOs and qualitatively considers the electron redistribution channels of categories 1 and 2, that is, the extra charges and the major Sb → Au redistribution of three electrons. In such a zeroth order picture, the all-metal sandwich can be formulated as $[\text{Sb}_3^{1.5+}\text{Au}_3^{3-}\text{Sb}_3^{1.5+}]^{3-}$ or $[\text{Sb}_3^0\text{Au}_3^{3-}\text{Sb}_3^0]$, where the layers are in formal charge states of Sb₃⁰ and Au₃³⁻. To reach the final, effective charge states of approximately Sb₃^{1.5-} and Au₃⁰, one has to go beyond the zeroth order picture and take into account the processes of categories 3 and 4.

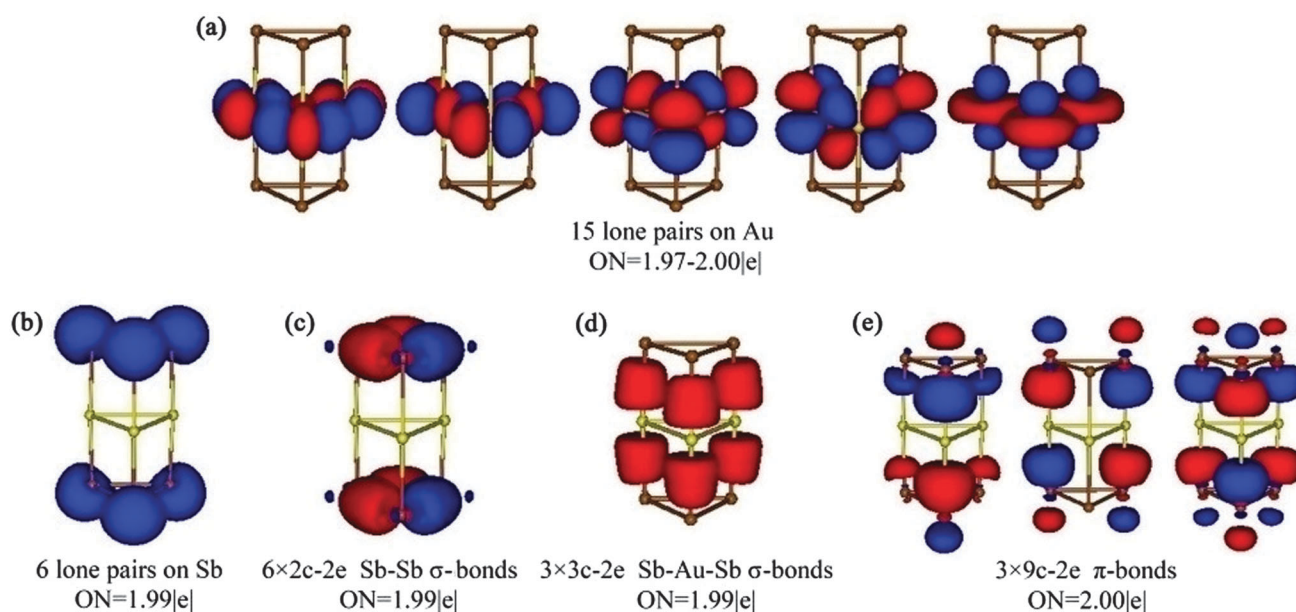


Fig. 5 The AdNDP bonding pattern for D_{3h} $[\text{Sb}_3\text{Au}_3\text{Sb}_3]^{3-}$. Occupation numbers (ONs) are shown.

with the value of n ranging from one to the total number of atoms in the molecule. AdNDP thus recovers the classical Lewis bonding elements (lone-pairs and 2c–2e bonds), as well as nonclassical delocalized nc –2e bonds. The AdNDP bonding pattern of $[\text{Sb}_3\text{Au}_3\text{Sb}_3]^{3-}$ is presented in Fig. 5. Not surprisingly, it successfully recovers 15 Au d^{10} lone-pairs (Fig. 5(a)) and 6 Sb $5s^2$ lone-pairs (Fig. 5(b)), whose 21 CMOs are shown in Fig. 2. Furthermore, it also recovers 6 Sb–Sb 2c–2e p_σ bonds (Fig. 5(c)) as well as 3 delocalized Sb 5p based π bonds (Fig. 5(e)); these correspond to the CMOs shown in Fig. 3(a) and (c), respectively.

Interestingly, the AdNDP data reveal three Sb–Au–Sb 3c–2e σ bonds with a nearly perfect occupation number (ON) of 1.99 $|e|$, as illustrated in Fig. 5(d). Note that, of all 33 CMOs for the sandwich complex (Fig. 2 and 3), one cannot identify even one CMO that is primarily responsible for the edge Sb–Au bonding. To reveal three Sb–Au–Sb 3c–2e σ bonds is thus a bit of a surprise. Yet this is exactly a virtualization of the complicated and quantitative data of electron donation and back-donation processes as presented in Tables 2 and 3. It is remarkable to be able to extract the essence relevant to the edge Sb–Au–Sb bonding from some 17 CMOs and synthesize them into three well-defined Sb–Au–Sb 3c–2e σ bonds. This represents an intriguing collective effect, which holds the key to the interlayer bonding in this all-metal sandwich system. One may suggest that, for example, HOMO–17 and HOMO–14/HOMO–14' (Fig. 2(b)) should help account for these edge bonds. However, these specific CMOs are actually part of the Au d^{10} lone-pairs. They contribute to the redistribution as little as $\sim 0.6 |e|$ in total from Au_3 to the Sb–Au–Sb edges (Table 3), that is, only $\sim 10\%$ for the edge bonds. The three Sb–Au–Sb 3c–2e σ bonds also approximately rationalize the calculated Sb–Au Wiberg bond order (0.71 at the PBE0/aug-cc-pVTZ-pp level; Table 2).

4. Conclusions

We have presented a density-functional theory study on the structural and electronic properties and chemical bonding of the recently synthesized $[\text{Sb}_3\text{Au}_3\text{Sb}_3]^{3-}$ cluster, the first all-metal aromatic sandwich. This triangular prismatic sandwich is viewed as a 24-electron system, being intrinsically electron-deficient for its six Sb–Sb, three Au–Au, and six Sb–Au links. Canonical molecular orbital (CMO) analyses suggest that the cluster may be approximately formulated as $[\text{Sb}_3^{1.5+}\text{Au}_3^{3-}\text{Sb}_3^{1.5+}]^{3-}$ in a zeroth order model, in which the metal centers are in formal Sb^0 and Au^- charge states. However, the actual bonding in the system is far more sophisticated. As many as 17 CMOs out of 33 in total contribute markedly to $\text{Sb} \rightarrow \text{Au}$ donation and $\text{Sb} \leftarrow \text{Au}$ back-donation, which are characteristic of covalent bonding. These processes effectively redistribute electrons in between the $\text{Sb}_3/\text{Au}_3/\text{Sb}_3$ layers of the sandwich, as well as from the metal layers to the interlayer Sb–Au–Sb edges. The collective effect of the processes is to result in the effective $\text{Sb}^{0.5-}$ and Au^0 charge states, which differ substantially from those in the zeroth order model. The inter-layer bonding in the sandwich is described and virtualized as

three Sb–Au–Sb three-center two-electron σ bonds according to the AdNDP analyses, despite the fact that none of such bonds can be traced back to the CMOs. The collective bonding effect from some 17 CMOs is remarkable and underlies the structure and the stability of $[\text{Sb}_3\text{Au}_3\text{Sb}_3]^{3-}$ as a unique all-metal aromatic sandwich.

Acknowledgements

This work was supported by the National Natural Science Foundation of China (21573138), the State Key Laboratory of Quantum Optics and Quantum Optics Devices (KF201402), and the Natural Science Foundation of Shandong Province (ZR2014BL011).

References

- 1 G. Wilkinson, M. Rosenblum, M. C. Whiting and R. B. Woodward, *J. Am. Chem. Soc.*, 1952, **74**, 2125.
- 2 E. O. Fischer and W. Z. Pfab, *Z. Naturforsch., B: J. Chem. Sci.*, 1952, **7**, 377.
- 3 A. Streitwieser, Jr. and U. Müller-Westerhoff, *J. Am. Chem. Soc.*, 1968, **90**, 7364.
- 4 (a) G. de Lauzon, B. Deschamps, J. Fischer, F. Mathey and A. Mitschler, *J. Am. Chem. Soc.*, 1980, **102**, 994; (b) A. Jabri, I. Korobkov, S. Gambarotta and R. Duchateau, *Angew. Chem., Int. Ed.*, 2007, **46**, 6119; (c) I. Vidyaratne, G. B. Nikiforov, S. I. Gorelsky, S. Gambarotta, R. Duchateau and I. Korobkov, *Angew. Chem., Int. Ed.*, 2009, **48**, 6552.
- 5 E. Urnèžius, W. W. Brennessel, C. J. Cramer, J. E. Ellis and P. v. R. Schleyer, *Science*, 2002, **295**, 832.
- 6 T. Murahashi, M. Fujimoto, M. Oka, Y. Hashimoto, T. Uemura, Y. Tatsumi, Y. Nakao, A. Ikeda, S. Sakaki and H. Kurosawa, *Science*, 2006, **313**, 1104.
- 7 T. Murahashi, Y. Hashimoto, K. Chiyoda, M. Fujimoto, T. Uemura, R. Inoue, S. Ogoshi and H. Kurosawa, *J. Am. Chem. Soc.*, 2008, **130**, 8586.
- 8 T. Murahashi, R. Inoue, K. Usui and S. Ogoshi, *J. Am. Chem. Soc.*, 2009, **131**, 9888.
- 9 (a) T. Murahashi, M. Fujimoto, Y. Kawabata, R. Inoue, S. Ogoshi and H. Kurosawa, *Angew. Chem., Int. Ed.*, 2007, **46**, 5440; (b) T. Murahashi, K. Usui, R. Inoue, S. Ogoshi and H. Kurosawa, *Chem. Sci.*, 2011, **2**, 117.
- 10 (a) Y. Tatsumi, K. Shirato, T. Murahashi, S. Ogoshi and H. Kurosawa, *Angew. Chem., Int. Ed.*, 2006, **45**, 5799; (b) T. Murahashi, N. Kato, T. Uemura and H. Kurosawa, *Angew. Chem., Int. Ed.*, 2007, **46**, 35092; (c) Y. Tatsumi, T. Murahashi, M. Okada, S. Ogoshi and H. Kurosawa, *Chem. Commun.*, 2008, 477; (d) T. Murahashi, Y. Mino, K. Chiyoda, S. Ogoshi and H. Kurosawa, *Chem. Commun.*, 2008, 4061; (e) T. Murahashi, K. Takase, M. Oka and S. Ogoshi, *J. Am. Chem. Soc.*, 2011, **133**, 14908; (f) T. Murahashi, K. Shirato, A. Fukushima, K. Takase, T. Suenobu, S. Fukuzumi, S. Ogoshi and H. Kurosawa, *Nat. Chem.*, 2012, **4**, 52; (g) T. Murahashi, S. Kimura, K. Takase, S. Ogoshi and K. Yamamoto, *Chem. Commun.*, 2013, **49**, 4310; (h) T. Murahashi, K. Takase,

- K. Usui, S. Kimura, M. Fujimoto, T. Uemura, S. Ogoshi and K. Yamamoto, *Dalton Trans.*, 2013, **42**, 10626.
- 11 J. M. Mercero and J. M. Ugalde, *J. Am. Chem. Soc.*, 2004, **126**, 3380.
- 12 M. Lein, J. Frunzke and G. Frenking, *Inorg. Chem.*, 2003, **42**, 2504.
- 13 Z. Li, W. Wu and S. Li, *J. Mol. Struct.: THEOCHEM*, 2009, **908**, 73.
- 14 A. E. Kuznetsov, H. J. Zhai, L. S. Wang and A. I. Boldyrev, *Inorg. Chem.*, 2002, **41**, 6062.
- 15 X. Li, A. E. Kuznetsov, H. F. Zhang, A. I. Boldyrev and L. S. Wang, *Science*, 2001, **291**, 859.
- 16 X. Li, H. F. Zhang, L. S. Wang, A. E. Kuznetsov, N. A. Cannon and A. I. Boldyrev, *Angew. Chem., Int. Ed.*, 2001, **40**, 1867.
- 17 A. I. Boldyrev and L. S. Wang, *Chem. Rev.*, 2005, **105**, 3716.
- 18 E. Maslowsky, *Coord. Chem. Rev.*, 2011, **255**, 2746.
- 19 F. X. Pan, L. J. Li, Y. J. Wang, J. C. Guo, H. J. Zhai, L. Xu and Z. M. Sun, *J. Am. Chem. Soc.*, 2015, **137**, 10954.
- 20 A. P. Sergeeva and A. I. Boldyrev, *Phys. Chem. Chem. Phys.*, 2010, **12**, 12050.
- 21 D. Y. Zubarev and A. I. Boldyrev, *Phys. Chem. Chem. Phys.*, 2008, **10**, 5207.
- 22 P. Hohenberg and W. Kohn, *Phys. Rev. B*, 1964, **136**, 864.
- 23 J. P. Perdew, K. Burke and M. Ernzerhof, *Phys. Rev. Lett.*, 1996, **77**, 3865.
- 24 J. P. Perdew, K. Burke and M. Ernzerhof, *Phys. Rev. Lett.*, 1997, **78**, 1396.
- 25 P. J. Hay and W. R. Wadt, *J. Chem. Phys.*, 1985, **82**, 270.
- 26 P. J. Hay and W. R. Wadt, *J. Chem. Phys.*, 1985, **82**, 299.
- 27 F. Weigend and R. Ahlrichs, *Phys. Chem. Chem. Phys.*, 2005, **7**, 3297.
- 28 R. A. Kendall, T. H. Dunning and R. J. Harrison, *J. Chem. Phys.*, 1992, **96**, 6796.
- 29 E. D. Glendening, J. K. Badenhoop, A. E. Reed, J. E. Carpenter, J. A. Bohmann, C. M. Morales and F. Weinhold, *NBO 5.0*, Theoretical Chemistry Institute, University of Wisconsin, Madison, 2001.
- 30 M. J. Frisch, G. W. Trucks, H. B. Schlegel, G. E. Scuseria, M. A. Robb, J. R. Cheeseman, G. Scalmani, V. Barone, B. Mennucci, G. A. Petersson, H. Nakatsuji, M. Caricato, X. Li, H. P. Hratchian, A. F. Izmaylov, J. Bloino, G. Zheng, J. L. Sonnenberg, M. Hada, M. Ehara, K. Toyota, R. Fukuda, J. Hasegawa, M. Ishida, T. Nakajima, Y. Honda, O. Kitao, H. Nakai, T. Vreven, J. A. Montgomery, Jr., J. E. Peralta, F. Ogliaro, M. Bearpark, J. J. Heyd, E. Brothers, K. N. Kudin, V. N. Staroverov, R. Kobayashi, J. Normand, K. Raghavachari, A. Rendell, J. C. Burant, S. S. Iyengar, J. Tomasi, M. Cossi, N. Rega, J. M. Millam, M. Klene, J. E. Knox, J. B. Cross, V. Bakken, C. Adamo, J. Jaramillo, R. Gomperts, R. E. Stratmann, O. Yazyev, A. J. Austin, R. Cammi, C. Pomelli, J. W. Ochterski, R. L. Martin, K. Morokuma, V. G. Zakrzewski, G. A. Voth, P. Salvador, J. J. Dannenberg, S. Dapprich, A. D. Daniels, Ö. Farkas, J. B. Foresman, J. V. Ortiz, J. Cioslowski and D. J. Fox, *GAUSSIAN 09, Revision D.01*, Gaussian, Inc., Wallingford, CT, 2009.
- 31 See for example: S. D. Li, H. J. Zhai and L. S. Wang, *J. Am. Chem. Soc.*, 2008, **130**, 2573.
- 32 P. Pykkö and M. Atsumi, *Chem. – Eur. J.*, 2009, **15**, 12770.
- 33 P. Pykkö, *J. Phys. Chem. A*, 2015, **119**, 2326.
- 34 H. Schmidbaur, *Gold Bull.*, 2000, **33**, 3.
- 35 P. Pykkö, *Angew. Chem., Int. Ed.*, 2004, **43**, 4412.
- 36 H. Schmidbaur and A. Schier, *Chem. Soc. Rev.*, 2008, **37**, 1931.
- 37 S. Sculfort and P. Braunstein, *Chem. Soc. Rev.*, 2011, **40**, 2741.
- 38 Since the PBE0 and B3LYP methods are known to be highly complementary with each other, the fact that both methods generate the same trend for the energy gap against the size of the basis set suggests that the trend is mainly due to the basis set. A logic conclusion is that the PBE0/aug-cc-pVTZ-pp data should be considered to be most reliable (see Section 2). Nonetheless, it remains to be benchmarked how well the PBE0/aug-cc-pVTZ-pp level of theory works in terms of calculating the energy gap for semiconducting systems, which is beyond the scope of this work.
- 39 We have performed calculations of the HOMO–LUMO gap for the $[\text{Pd}_4(\mu_4\text{-C}_9\text{H}_9)(\mu_4\text{-C}_8\text{H}_8)]^+$ system⁸ as well, and the trend is the same. At the PBE0 level, the calculated energy gap amounts to 2.90, 3.01, and 0.68 eV with the LANL2DZ, def2-TZVP, aug-cc-pVTZ-pp basis sets, respectively. For comparison, the corresponding data are 2.49, 2.58, and 0.62 eV at the B3LYP level with the same basis sets.
- 40 N. C. Baird, *J. Am. Chem. Soc.*, 1972, **94**, 4941.
- 41 Note that π aromaticity in the all-metal $[\text{Sb}_3\text{Au}_3\text{Sb}_3]^{3-}$ sandwich complex is manifested in the text on the bases of a number of “standard” criteria: the CMO analysis, electron counting according to the reversed $4n$ Hückel rule, AdNDP analysis, NICS, and bond distance equalization (structural criterion). Among these, the CMO analysis is the most fundamental. AdNDP as an extension of the NBO analysis is useful, whereas NBO itself does not work for such a system because it cannot go beyond $3c\text{--}2e$ bonds.
- 42 P. v. R. Schleyer, C. Maerker, A. Dransfeld, H. Jiao and N. J. R. V. E. Hommes, *J. Am. Chem. Soc.*, 1996, **118**, 6317.
- 43 Z. F. Chen, C. S. Wannere, C. Corminboeuf, R. Puchta and P. v. R. Schleyer, *Chem. Rev.*, 2005, **105**, 3842.